Bioresource Technology 458 (2026) 135071

Contents lists available at ScienceDirect

Bioresource Technology

journal homepage: www.elsevier.com/locate/biortech

# Accelerating yeast adaptation: harnessing thermal stress for genomic diversification and thermotolerance in *Yarrowia lipolytica*

Min He [a,b,1], Ke Zhang [c,1], Qian-Xin Hong [d], Yuan-Chun Fang [b], Yuan-Ru Xiong [b], Ye-Ke Wang [c], Dao-Qiong Zheng [a,b,*]

[a] Hainan Institute, Zhejiang University, Sanya 572000, China
[b] Ocean College, Zhejiang University, Zhoushan 316021, China
[c] College of Life Science, Zhejiang University, Hangzhou 310058, China
[d] Marine Science and Technology College, Zhejiang Ocean University, Zhoushan 316021, China

## HIGHLIGHTS

- Thermal stress drastically elevates genomic instability in *Y. lipolytica*.
- Heat-induced mutagenesis arises from impaired replication fidelity.
- Heat stress triggers severe telomere instability and chromosomal rearrangements.
- Knockout of *YALI1_B03404g* enhances thermotolerance and suppresses dimorphism.

## GRAPHICAL ABSTRACT

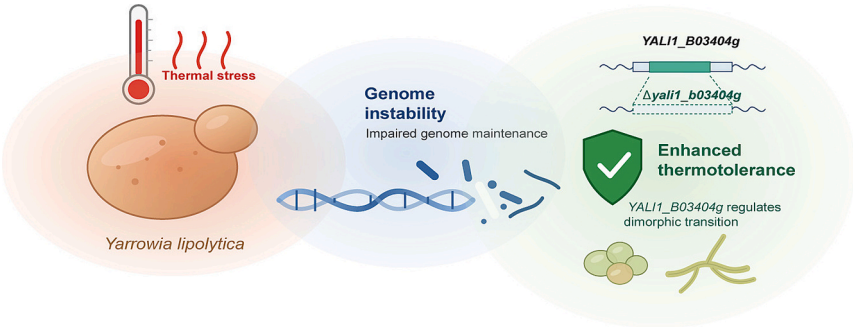


## ARTICLE INFO

*Keywords:*
Yeast
Thermotolerance
DNA repair
Dimorphism
Adaptive evolution

## ABSTRACT

Temperature sensitivity remains a significant bottleneck in the industrial application of the oleaginous yeast *Yarrowia lipolytica*. While adaptive evolution and metabolic engineering have produced thermotolerant variants, the impact of thermal stress on the genomic integrity of this non-conventional yeast remains poorly understood. Here, we employed a mutation accumulation framework coupled with whole-genome sequencing to characterize the mutational landscape of *Y. lipolytica* at 37°C. We observed a 29- and 68-fold increase in single-nucleotide variations and small insertions/deletions, respectively, compared to optimal growth conditions (30°C). Mechanistic analysis revealed that this mutagenicity is independent of error-prone translesion and nonhomologous end joining pathways; instead, thermal stress overwhelms the replicative fidelity of DNA polymerases and the mismatch repair system. Furthermore, long-read sequencing identified severe telomere instability and large-scale chromosomal rearrangements, including the frequent formation of circular chromosomes and terminal fusions. Lastly, functional genomics revealed *YALI1_B03404g* to be a key negative regulator of heat resistance. Its deletion substantially enhances thermotolerance, a phenotype potentially mediated through the modulation of yeast-to-

* Corresponding author at: Room 377, Marine Science Building, No.1 Zheda Road, Dinghai District, Zhoushan, Zhejiang 316021, China.
*E-mail addresses:* 12434005@zju.edu.cn (M. He), zhangke726@zju.edu.cn (K. Zhang), 19818001256@163.com (Q.-X. Hong), fangyuanchunde163@163.com (Y.-C. Fang), xyr990126@163.com (Y.-R. Xiong), yekewang@126.com (Y.-K. Wang), zhengdaoqiong@zju.edu.cn (D.-Q. Zheng).
[1] These authors contributed equally to this study.

https://doi.org/10.1016/j.biortech.2026.135071
Received 1 April 2026; Received in revised form 26 May 2026; Accepted 2 June 2026
Available online 6 June 2026

hypha transitions. Collectively, our findings enhance the understanding of genomic evolution in non-conventional yeasts under thermal stress and offer a valuable framework for developing robust industrial strains.

## 1. Introduction

As unicellular organisms, yeasts frequently encounter diverse environmental stressors in both their natural habitats and industrial settings. Among these, elevated temperature represents a primary challenge to cellular homeostasis, often resulting in impaired protein folding, compromised membrane integrity, and disrupted metabolic flux (Jenkins et al., 1997; Pereira et al., 2018). In the model yeast *Saccharomyces cerevisiae*, several conserved mechanisms of thermotolerance have been characterized, including the induction of heat shock proteins (HSPs) (Xu et al., 2019), the accumulation of cytoprotective trehalose (Elliott et al., 1996), the assembly of stress granules (Grousl et al., 2013), the modulation of membrane lipid composition (Carratù et al., 1996), and the activation of robust antioxidant defense systems (Davidson et al., 1996).

Beyond immediate physiological perturbations, heat stress exerts a profound impact on genome stability. Cultivation of *S. cerevisiae* at supra-optimal temperatures (38-42°C) has been shown to induce a fourfold increase in single-nucleotide variations (SNVs) (Huang et al., 2018). The SNVs were distributed across the genome without obvious mutation hotspots (Huang et al., 2018). Moreover, severe thermal shock (52°C) can trigger a dramatic rise in loss of heterozygosity (LOH) and a 100-fold surge in chromosomal aberrations, including large-scale rearrangements and aneuploidy (Shen et al., 2020). Recent evidence in *Cryptococcus neoformans* also highlights the activation of transposable elements at 37°C as a major driver of genomic diversity under thermal stress (Gusa et al., 2023). This study revealed that the T1 DNA transposon transposed at both 30°C and 37°C, showing a strong bias for intergenic regions; the Tcn12 retrotransposon integrated primarily within genes exclusively at 37°C; and the Cnl1 retrotransposon exhibited dramatic copy-number amplification in subtelomeric regions at 37°C (Gusa et al., 2023). Despite these insights, the impact of heat stress on the genomic landscapes of non-conventional yeasts remains poorly understood.

*Yarrowia lipolytica*, an oleaginous yeast renowned for its metabolic versatility, is a premier chassis for biotechnological applications. Its ability to utilize hydrophobic substrates and produce high-value lipids, organic acids, and enzymes has made it a cornerstone of microbial cell factories (Qin et al., 2025; Yook et al., 2025; Zhou et al., 2025). However, its industrial wider adoption is hindered by inherent temperature sensitivity; while it grows optimally at 28-30°C, growth is severely inhibited above 34°C (Bankar et al., 2009). This thermal constraint necessitates the use of intensive cooling systems during large-scale fermentation, which significantly escalates operational costs (Qiu et al., 2021). While strategies such as adaptive laboratory evolution and genetic engineering have been employed to bolster thermotolerance—identifying roles for thiamine metabolism (Qiu et al., 2021), HSPs (Zhang et al., 2022), gene *HRC1-3* (Liu and Cheng, 2023), antioxidant enzymes like catalase Ctt1 (Liang et al., 2023), and ubiquitin ligase gene *RSP5* (Shahsavarani et al., 2012; Wang et al., 2020) in Y. lipolytica improved its heat resistance—the frequency and spectrum of heat-induced genomic variations in *Y. lipolytica* remain elusive. Furthermore, the specific genetic mutations that facilitate thermal adaptation in this species have not been systematically mapped.

In this study, we employed a mutation accumulation (MA) experiment coupled with high-throughput whole-genome sequencing to systematically characterize the impact of thermal stress on the genomic integrity of *Y. lipolytica*. Our findings demonstrate that elevated temperatures exert potent mutagenic pressure, significantly accelerating the accumulation of both point mutations and large-scale chromosomal rearrangements. Beyond cataloging these variations, we investigated the underlying genetic mechanisms and, through targeted genetic engineering, confirmed the functional significance of specific genomic alterations in conferring thermotolerance. Notably, the deactivation of the gene *YALI1_B03404g* was found to significantly enhance cellular resistance to heat stress. Collectively, these results provide novel insights into the genetic landscape of thermal adaptation in *Y. lipolytica* and offer precise molecular targets for the development of robust, thermotolerant microbial cell factories for industrial applications.

## 2. Materials and methods

### 2.1. Strain and medium

All *Y. lipolytica* strains used in this study are detailed in Table 1. The wild-type *Y. lipolytica* strain W29 (ATCC 20460) served as the parental strain for the MA experiments. For genetic engineering and functional validation, the laboratory strain PO1f was utilized as the starting background (Table 1). To facilitate efficient genome editing via the CRISPR/Cas9 system, a *CAS9* expression cassette was integrated into the

**Table 1**
Yeast strains used in this study.

| Strain | Genotype | Source |
|---|---|---|
| W29 | *MatA* | ATCC 20,460 |
| PO1f | *MatA leu2-270 ura3-302 xpr2-322 axp1-2* | (Xiong et al., 2025) |
| PPY3 | *MatA leu2-270 ura3-302 xpr2-32 axp1-2 int::CAS9-LEU2 LYS9-Δ* | (Xiong et al., 2025) |
| PPF | *MatA leu2-270 ura3-302 xpr2-322 axp1-2 int::CAS9-LEU2 LYS9-Δ int::LYS9* | (Xiong et al., 2025) |
| PPW | *MatA leu2-270 ura3-302 xpr2-322 axp1-2 int::CAS9-LEU2 LYS9-Δ int::LYS9 int::URA3* | this work |
| PPY3Δ*ku70* | *MatA leu2-270 ura3-302 xpr2-32 axp1-2 int::CAS9-LEU2 LYS9-Δ Δku70 int::LYS9* | (Xiong et al., 2025) |
| PPY3Δ*rad30* | *MatA leu2-270 ura3-302 xpr2-32 axp1-2 int::CAS9-LEU2 LYS9-Δ Δrad30 int::LYS9* | (Xiong et al., 2025) |
| PPY3Δ*rev1* | *MatA leu2-270 ura3-302 xpr2-32 axp1-2 int::CAS9-LEU2 LYS9-Δ Δrev1 int::LYS9* | (Xiong et al., 2025) |
| PPY3Δ*rev3* | *MatA leu2-270 ura3-302 xpr2-32 axp1-2 int::CAS9-LEU2 LYS9-Δ Δrev3 int::LYS9* | (Xiong et al., 2025) |
| PPY3Δ*F00184g* | *MatA leu2-270 ura3-302 xpr2-32 axp1-2 int::CAS9-LEU2 LYS9-Δ Δmsh2 int::LYS9* | this work |
| PPY3Δ*B29266g* | PPY3 Δ*yali1_b29266g* | this work |
| PPY3Δ*D24026g* | PPY3 Δ*yali1_d24026g::LYS9* | this work |
| PPY3Δ*E15211g* | PPY3 Δ*yali1_e15211g::LYS9* | this work |
| PPY3Δ*B11983g* | PPY3 Δ*yali1_b11983g::LYS9* | this work |
| PPFΔ*B03404g* | PPY3 Δ*yali1_b03404g int::LYS9* | this work |
| PPY3Δ*D24308g* | PPY3 Δ*yali1_d24308g* | this work |
| PPFΔ*F00184g* | PPF Δ*yali1_ f00184g int::URA3* | this work |
| PPFΔ*C24891g* | PPF Δ*yali1_c24891g int::URA3* | this work |
| PPFΔ*C24891g* ΔB03404g | PPF Δ*yali1_c24891g* Δ*yali1_b03404g int::URA3* | this work |
| PPFB03404YFP | PPF Δ*yali1_b03404g int::YFP-YALI1_B03404g* | this work |
| PPFB03404g | PPF *int::YALI1_B03404g* | this work |
| PPFΔ2-131 | PPF Δ*yali1_b03404g int::YALI1_B03404gΔ2–131* | this work |
| PPFΔ151-222 | PPF Δ*yali1_b03404g int::YALI1_B03404gΔ151–222* | this work |
| PPFΔ545-607 | PPF Δ*yali1_b03404g int::YALI1_B03404gΔ545–607* | this work |

PO1f genome, yielding the strain PPF (*MATA leu2-270 ura3-302 xpr2-322 axp1-2* int::*CAS9-LEU2 LYS9-Δ int::LYS9*) (Xiong et al., 2025). The oligonucleotides employed for strain construction are provided in Dataset S1. Routine cultivation was performed in YPD medium (10 g/L yeast extract, 20 g/L peptone, and 20 g/L dextrose).

### 2.2. Mutation accumulation experiment of *Y. lipolytica* strains

To explore the genomic alterations in *Y. lipolytica* at heat conditions, we subcultured 10–20 independent isolates of the *Y. lipolytica* strain on solid YPD medium for 10–20 cycles at 35°C (PO1f background) or 37°C (W29 background). For each cycle, a colony on a YPD plate was randomly selected and streaked onto a new YPD plate, followed by incubation at 35°C or 37°C for 3 days. By counting all cells in a clone, we calculated that approximately 25 cell divisions occurred from a single cell to the formed clone.

### 2.3. DNA extraction and whole genome sequencing

DNA extraction and next-generation sequencing were performed as described in our recent studies (Xiong et al., 2025; Yan et al., 2025). Briefly, genomic DNA was extracted from approximately $1 \times 10^8$ Y. lipolytica cells using the commercial DNA extraction kit (Apostle MiniGenomics). DNA libraries were constructed using the VAHTS® Universal Plus kit (Vazyme) with MGI Adapter Set 8. Following ligation, libraries were circularized using the VAHTS® Circularization Kit. Sequencing was performed on an MGISEQ-2000 platform in $2 \times 150$ bp paired-end mode, following the generation of DNA nanoballs (DNBs) with the MGISEQ-2000RS kit. Raw reads were processed using FastQC for quality control and Trimmomatic for adapter removal and quality trimming (Phred score threshold = 20) (Bolger et al., 2014).

### 2.4. Detection of SNVs and small insertions and deletions (InDels)

Clean reads were mapped to the *Y. lipolytica* reference genome (RefSeq accession: GCF_001761485.1) using the BWA-MEM algorithm with default parameters (Li, 2013). The resulting alignments were processed using SAMtools to generate sorted BAM files and subsequent mpileup formats (Li et al., 2009). SNVs and InDels were identified using VarScan (Koboldt et al., 2012), with the mpileup files as input. To assess the functional impact of these mutations on protein-coding sequences, SnpEff was employed utilizing a pre-annotated *Y. lipolytica* genomic database (Cingolani et al., 2012). Mutation rates were calculated as follows: the number of SNVs or InDels/the number of base pairs of the genome of *Y. lipolytica*/the total number of cell divisions.

### 2.5. Analysis of DNA copy number variations

The sequencing coverage (DNA copy number) of the genomes of *Y. lipolytica* isolates was calculated using Bedtools, with the sorted BAM files as input (Quinlan and Hall, 2010). The coverage for each sample was calculated using with a bin size of 1000 bp and a sliding step of 500 bp.

### 2.6. RNA-seq of Y. lipolytica strains

Yeast cells were cultured in 25 mL of YPD medium at 30°C with constant shaking until reaching mid-log phase ($OD_{600} = 1$). The cultures were then incubated at either 30°C (control) or transiently shifted to 37°C for 2 h. Subsequently, cells were harvested by centrifugation at 4,000 g for 5 min. Total RNA was extracted from *Y. lipolytica* cultures (three independent cultures for each strain) using the RNeasy Mini Kit (Qiagen) according to the manufacturer's instructions. RNA libraries were prepared using the NEBNext Ultra II RNA Library Prep Kit (New England Biolabs), following the manufacturer's protocol. The RNA-seq libraries were sequenced on an Illumina NovaSeq 6000 platform, generating paired-end reads (150 bp). Raw sequence data in FASTQ format were processed using FastQC to assess read quality, followed by trimming and filtering using Trimmomatic to remove low-quality reads and adapter sequences (Bolger et al., 2014). The clean reads were aligned to the *Y. lipolytica* genome using the STAR aligner (Dobin et al., 2013). Gene expression levels were quantified by counting reads mapped to each gene using featureCounts (Liao et al., 2014). Differential gene expression analysis was performed using the DESeq2 package in R (Love et al., 2014).

### 2.7. Genetic manipulation

Gene deletion in *Y. lipolytica* PPF (a *CAS9* gene was integrated on its genome in our previous study; Table 1) was performed using the dual-sgRNA expression plasmid pU2gR (Xiong et al., 2025) (Fig. 1A). This system facilitates the simultaneous introduction of two DNA double-strand breaks within a single target gene to enhance knockout efficiency. Target-specific sgRNA sequences were identified using the CRISPOR web tool and subsequently incorporated into the pU2gR backbone via PCR, utilizing primers with 5′ overhangs containing the spacer sequences. Primer sequences are shown in Dataset S1.

To investigate the subcellular localization of protein Yali1_b03404p, we constructed the expression vector pNB03404_YFP (Fig. 1B). This plasmid encodes an *N*-terminal YFP-fusion protein under the control of the synthetic hybrid promoter P2_4UASxpr-TEF (Fig. 1B). The vector also harbors the *URA3* selection marker and retrotransposon-derived repetitive sequences (Zeta) derived from plasmid GGE067 (https://www.addgene.org/120784/) for stable genomic integration. To delineate the functional domains of Yali1_b03404p, three in-frame internal deletion variants were generated (Fig. 1C). These variants lacked the coding regions for amino acids 2–131, 151–222, and 545–607, respectively, yielding the plasmids pUZB03404g_d2-131a, pUZB03404g_d151-222a, and pUZB03404g_d545-607a. To generate the *YALI1_B03404g*-overexpressing strain, the Zeta_NotI-up-YALI1_B03404g-URA3-Zeta_NotI-down fragment was amplified from the previously constructed PUZB03404 plasmid and introduced into the wild-type strain PPF.

Above plasmid or PCR amplified integration cassettes (Zeta_NotI-up-B03404g_d2-131a-URA3-Zeta_NotI-down, Zeta_NotI-up-B03404g_d151-222a-URA3-Zeta_NotI-down, and Zeta_NotI-up-B03404g_d545-607a-URA3-Zeta_NotI-down) were transformed into *Y. lipolytica* strain using the standard ssDNA/PEG/LiAc method. Correct integration and gene disruptions were verified by locus-specific PCR and Sanger sequencing.

### 2.8. Statistical analysis

The 95% confidence intervals (CIs) for mutation rates were calculated based on a Poisson distribution. To assess the statistical significance of differences in mutation rates between spontaneous and heat-induced (mutagenic) conditions, the Wilcoxon rank-sum test (also known as the Mann-Whitney *U* test) was employed.

### 2.9. Data availability

The raw data of whole genome sequencing of *Y. lipolytica* isolates were deposited in the SRA database with the accession number of PRJNA1444363.

## 3. Results and discussion

### 3.1. Thermal stress severely compromises genomic stability in Y. lipolytica

When cultured in liquid YPD medium at 30°C, the wild-type *Y. lipolytica* strain W29 exhibited a maximal growth rate of 0.25 $h^{-1}$ (Fig. 2A). Exposure to an elevated temperature of 37°C resulted in a 65% reduction in the maximal growth rate and a concomitant decrease in

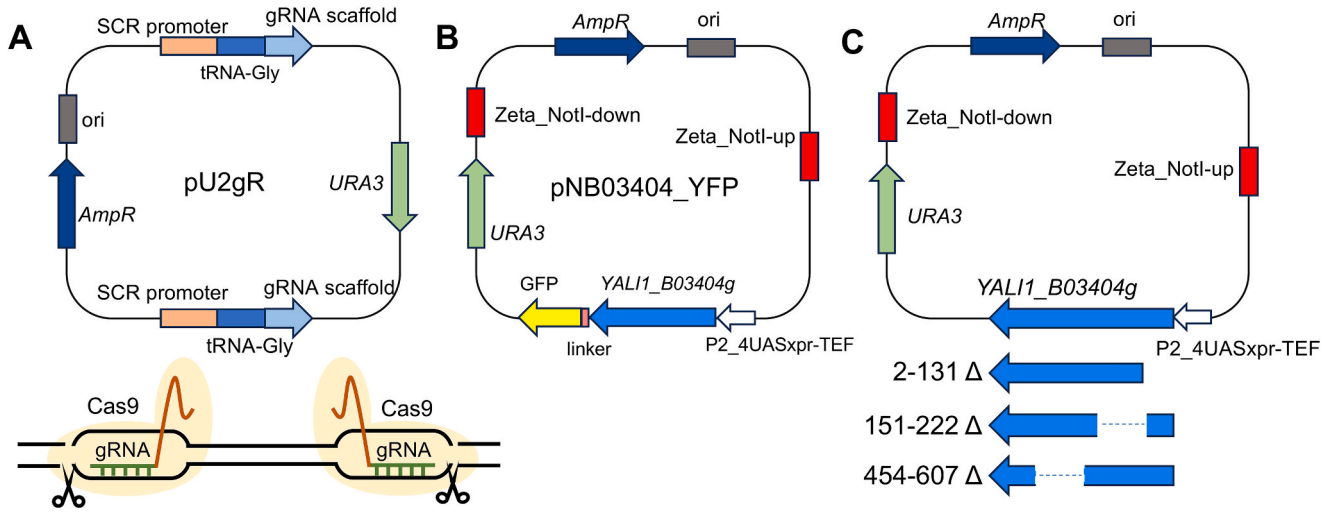


**Fig. 1.** Plasmid construction strategies for gene deletion and protein expression. (A) Schematic of plasmid pU2gR, designed for the simultaneous expression of dual gRNAs targeting a specific locus. (B) pNB03404_YFP is a vector for the expression of fluorescently tagged proteins. (C) Construction of *YALI1_B03404g* variants through the integration of partial ORF sequences into the pNB03404_YFP backbone.

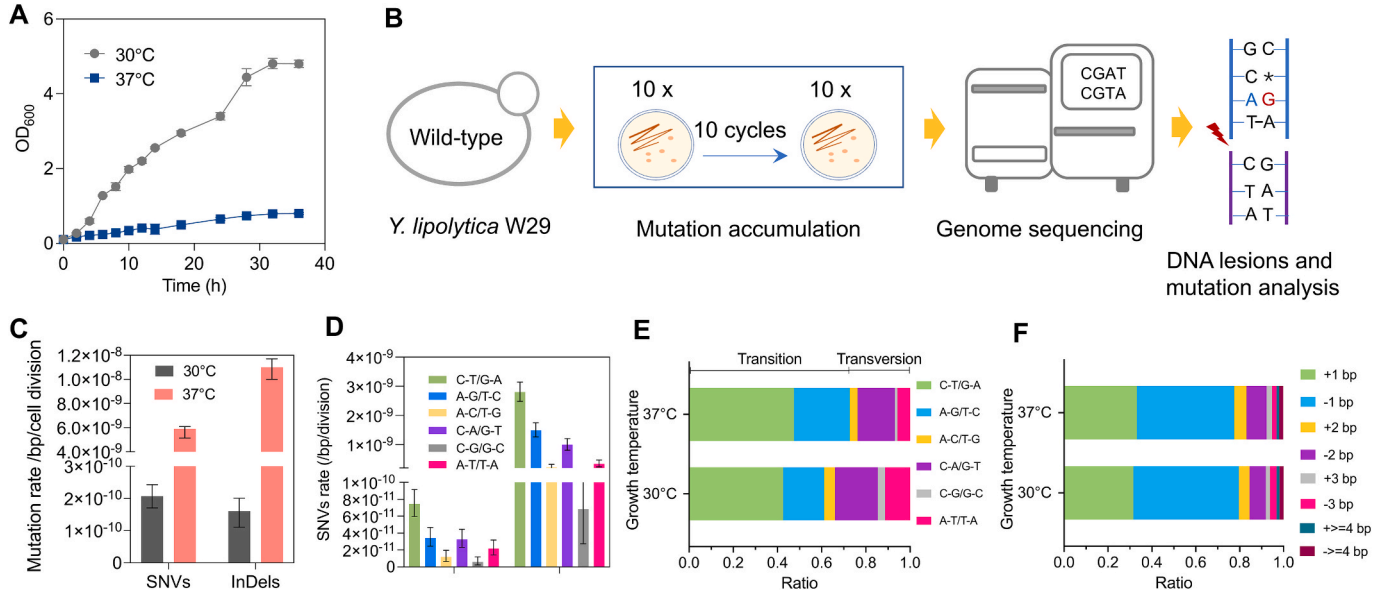


**Fig. 2.** Growth and mutation rates of *Y. lipolytica* strain at 30°C and 37°C. (A) Biomass formation of *Y. lipolytica* strain W29 incubated in 25 mL YPD at 30°C and 37°C. The initial $OD_{600}$ is of 0.05. (B) Mutation accumulation experiment and genome sequencing of *Y. lipolytica* strain W29. (C) The rates of SNVs and InDels of *Y. lipolytica* at 30°C (n = 21) and 37°C (n = 10). (D) The rate of each individual base substitution of *Y. lipolytica* at 30°C and 37°C. (E) The relative ratio of each type of base substitutions. (F) The relative ratio of each type of InDels.

biomass accumulation (Fig. 2A). To investigate whether high temperatures compromise genome integrity, we performed a MA experiment. Ten independent isolates of strain W29 were subcultured on YPD agar at 37°C for 20 serial passages (Fig. 2B). In parallel, 21 control isolates were maintained at 30°C for approximately 100 generations to accumulate a comparable number of mutations for statistical robustness (Xiong et al., 2025). Genomic DNA from all isolates was analyzed via whole-genome sequencing, yielding at least 2 Gb of high-quality reads per isolate. Reads were aligned to the *Y. lipolytica* reference genome to identify SNVs, InDels, and copy number variations (CNVs).

Among the 10 isolates subcultured at 37°C, we identified a total of 606 SNVs (Dataset S2). Based on a genome size of 20.5 Mb and an estimated 5,000 total cell divisions (calculated as 25 divisions/generation × 20 passages × 10 isolates), the rate of SNVs was determined to be $5.91 \times 10^{-9}$ per base pair per cell division. This represents a 29-fold increase compared to the rate observed at 30°C ($2.07 \times 10^{-10}$ per bp per division; Fig. 2B). Analysis of the mutational spectrum (Fig. 2C) revealed that the most prevalent substitution type at 37°C was C-to-T/G-to-A transitions, accounting for 47% of all heat-induced SNVs, a slight increase from the 43% observed at 30°C. The second most frequent type was A-to-G/*T*-to-C transitions (27% at 37°C vs. 19% at 30°C), indicating that transitions occur more frequently under thermal stress than at optimal temperatures ($P < 0.05$, Fisher's exact test). Regarding their functional impact, 34% of SNVs were located within coding regions, including 148 missense mutations and 4 nonsense mutations (Dataset S2).

Furthermore, we detected 1,132 InDels in the 37°C isolates (Dataset S3), corresponding to a rate of $1.1 \times 10^{-8}$ per bp per division. This signifies a 68-fold escalation over the spontaneous InDels rate at 30°C (Fig. 2D). The majority (78%) of heat-induced InDels were 1-bp events

occurring within mononucleotide or microsatellite repeats (Fig. 2E and Dataset S3), a pattern consistent with observations at 30°C (Xiong et al., 2025). These data suggest that high temperatures may compromise the fidelity of DNA polymerases, leading to increased replication slippage, or potentially impair the cellular capacity to repair such replication errors. Notably, 91% of InDels were localized to non-coding regions—a significantly higher proportion than that observed for SNVs. This disparity suggests that InDels within coding sequences are subject to more stringent purifying selection during subculturing.

Overall, our results showed that the level of base-substitution induction by high temperature is remarkably comparable to that achieved by traditional powerful mutagens, such as ultraviolet radiation and methane methylsulfonate in *Y. lipolytica* (Xiong et al., 2025). However, the mutagenic potency of high temperature toward InDels appears significantly superior to these chemical and physical agents. Given this high mutagenic efficiency and its distinct bias toward InDels—which are more likely to cause significant functional diversification—high temperature treatment emerges as an exceptionally cost-effective, accessible, and robust tool for industrial traits improvement.

### 3.2. Heat induced mutations are not dependent on translesion synthesis (TLS) and non-homologous end joining (NHEJ) pathways

To investigate the molecular origin of heat-induced mutations, we turned our attention to two major error-prone repair pathways: TLS and NHEJ. While TLS allows replication to bypass DNA damage via specialized polymerases (Rev1, Pol ζ, and Pol η) (Arbel et al., 2021; Yan et al., 2025), NHEJ resolves DSBs in a template-independent manner (Fraczek et al., 2018); both are known sources of SNVs and InDels. We hypothesized that if heat stress triggers DNA damage that is subsequently processed by these pathways, their deletion should alter the observed mutation spectrum or rate. To test this, we subjected the wild-type strain (PPF) and mutants lacking *KU70*, *REV1*, *REV3*, or *RAD30* to thermal stress at 35°C (the maximum permissive temperature for the PO1f background) for 10 cycles. Contrary to the hypothesis, whole genome sequencing analysis revealed that the loss of these key repair components did not significantly alter mutation frequencies (Fig. 3A). The SNVs rates in the Δ*ku70*, Δ*rev1*, Δ*rev3*, and Δ*rad30* backgrounds remained comparable to the parental strain (ranging from $8.8 \times 10^{-10}$ to $1.6 \times 10^{-9}$ vs. $1.3 \times 10^{-9}$ per base per division; $P > 0.05$) (Fig. 3A and Dataset S4). InDels rates were similarly unaffected across all genotypes (Fig. 3A and Dataset S4). These findings suggest that the mutagenic effect of high temperature in *Y. lipolytica* is independent of TLS-mediated lesion bypass and NHEJ-mediated break repair.

Previous studies have indicated that high temperatures can induce indirect stressors, such as the accumulation of reactive oxygen species, which potentially lead to oxidative base damage and DNA double-strand breaks (DSBs) (Habibi et al., 2022). Since the base excision repair (BER) pathway is the main mechanism repairing oxidative base damage, if BER were inhibited by thermal stress, one would expect a significant increase in SNVs without a concomitant surge in InDels frequency (Mitra et al., 2001). This scenario, however, is inconsistent with our observation of a marked elevation in InDels rates. Furthermore, while the TLS pathway typically introduces mutations during the bypass of damaged bases (Yan et al., 2025; Zheng et al., 2022), our results demonstrate that the loss of key components in either the TLS or NHEJ pathways does not alter the frequency under heat stress. These findings collectively suggest that oxidative damage and DSBs are not the primary genotoxic drivers of heat-induced mutagenesis in *Y. lipolytica*.

### 3.3. The fidelity of replicative DNA polymerases is jeopardized when Y. lipolytica is incubated under high temperature

DNA replication fidelity is primarily maintained by a dual-layered defense system: the proofreading activity of DNA polymerases and the post-replicative mismatch repair (MMR) pathway. Disrupting these mechanisms simultaneously elevates the rates of SNVs and InDels, typically with a more profound impact on InDels. Interestingly, in *Y. lipolytica*, high-temperature stress mirrors this pattern, inducing a more significant increase in InDels than in SNVs (Fig. 2C). This consistency led us to hypothesize that thermal stress may impair either the proofreading efficiency of DNA polymerases or the functional integrity of the MMR pathway.

To test this, we generated an *MSH2* deletion strain to completely abolish MMR activity and subjected it to mutation accumulation experiments at 30°C and 35°C. We reasoned that if heat-induced mutagenicity is purely a result of MMR inhibition, the mutation rate in the Δ*msh2* background would remain constant regardless of temperature. Conversely, if high temperatures continue to exacerbate mutation rates in the absence of MMR, it would suggest that thermal stress increases raw replication errors to a level that exceeds the repair capacity of the MMR system. Compared to the wild-type strain (PPF), the SNVs and InDels rates surged to $5.9 \times 10^{-9}$ (33-fold increase) and $1.1 \times 10^{-8}$ (117-fold increase) (Fig. 3B). When the temperature was raised to 35°C, the Δ*msh2* strain exhibited an additional 1-fold increase in both SNVs and InDels frequencies compared to its 30°C baseline (Fig. 3B). These findings indicate that heat-induced point mutations primarily stem from an overwhelming influx of replication errors that surpass the MMR system's corrective limit. While these data emphasize increased error generation, we cannot exclude the possibility that high temperatures also partially inhibit the enzymatic efficiency of MMR proteins. To experimentally delineate these two non-mutually exclusive mechanisms, future *in vitro* biochemical reconstruction assays are highly warranted. First, by measuring the error rates on single-stranded templates, researchers can calculate the exact temperature coefficient for base misincorporation and determine if elevated temperatures uncouple the polymerase activity from its 3′-5′ exonuclease proofreading capacity. Second, to measure MMR catalytic efficiency, pre-fabricated heteroduplex DNA substrates containing single, defined base–base mismatches can be incubated with the purified *Y. lipolytica* MMR machinery. Characterizing the endonuclease cleavage and exonuclease-mediated excision rates at different temperatures will allow for the determination of the MMR

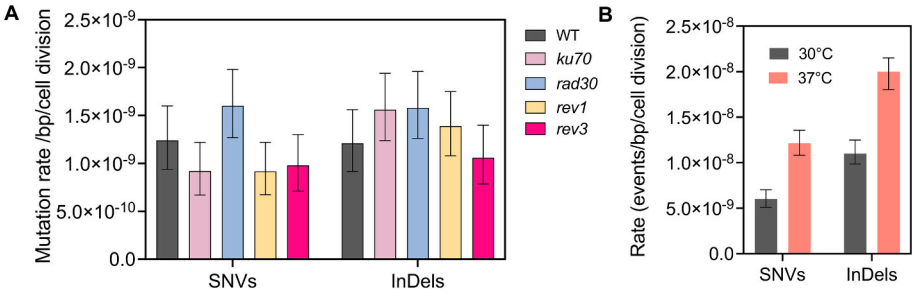


**Fig. 3.** Effect of DNA repair pathways on mutations rates of *Y. lipolytica*. (A) Comparison of SNVs and InDELs rates of the wild-type strain and the mutants lacking *KU70*, *REV1*, *REV3*, and *RAD30* grown at 37°C. (B) Effects of temperature on SNVs and InDels of wild-type strain and *msh2* mutant.

activity.

### 3.4. Heat stress stimulates telomere instability and chromosomal rearrangements in Y. lipolytica

By mapping sequencing reads to the *Y. lipolytica* reference genome and analyzing depth of coverage, we identified 12 large-scale (> 1 kb) CNVs events across the 10 isolates subcultured at 37°C (Fig. 4). The frequency of CNVs was calculated as $2.4 \times 10^{-3}$ events per genome per cell division, which is 16-fold of that in the wild-type strain (Xiong et al., 2025). Significant segmental duplications were detected, including a 1.05–1.26 Mb region on chromosome A and a 1.23–1.29 Mb region on chromosome E in strain W37-4 (Fig. 4A, B). Similarly, strain W37-5 exhibited a 492 kb duplication on chromosome E (Fig. 4C), while W37-10 harbored two duplicated segments on chromosome A (Fig. 4D). Conversely, a 15.8 kb interstitial deletion was identified on chromosome A in strain W37-4 (Fig. 4A). Beyond these internal rearrangements, subtelomeric regions were found to be hotspots for CNVs, characterized by terminal deletions and duplications in strains W37-5 and W37-6 (Fig. 4C, E).

To resolve the complex genomic architectures underlying these CNVs, we performed long-read sequencing of four representative

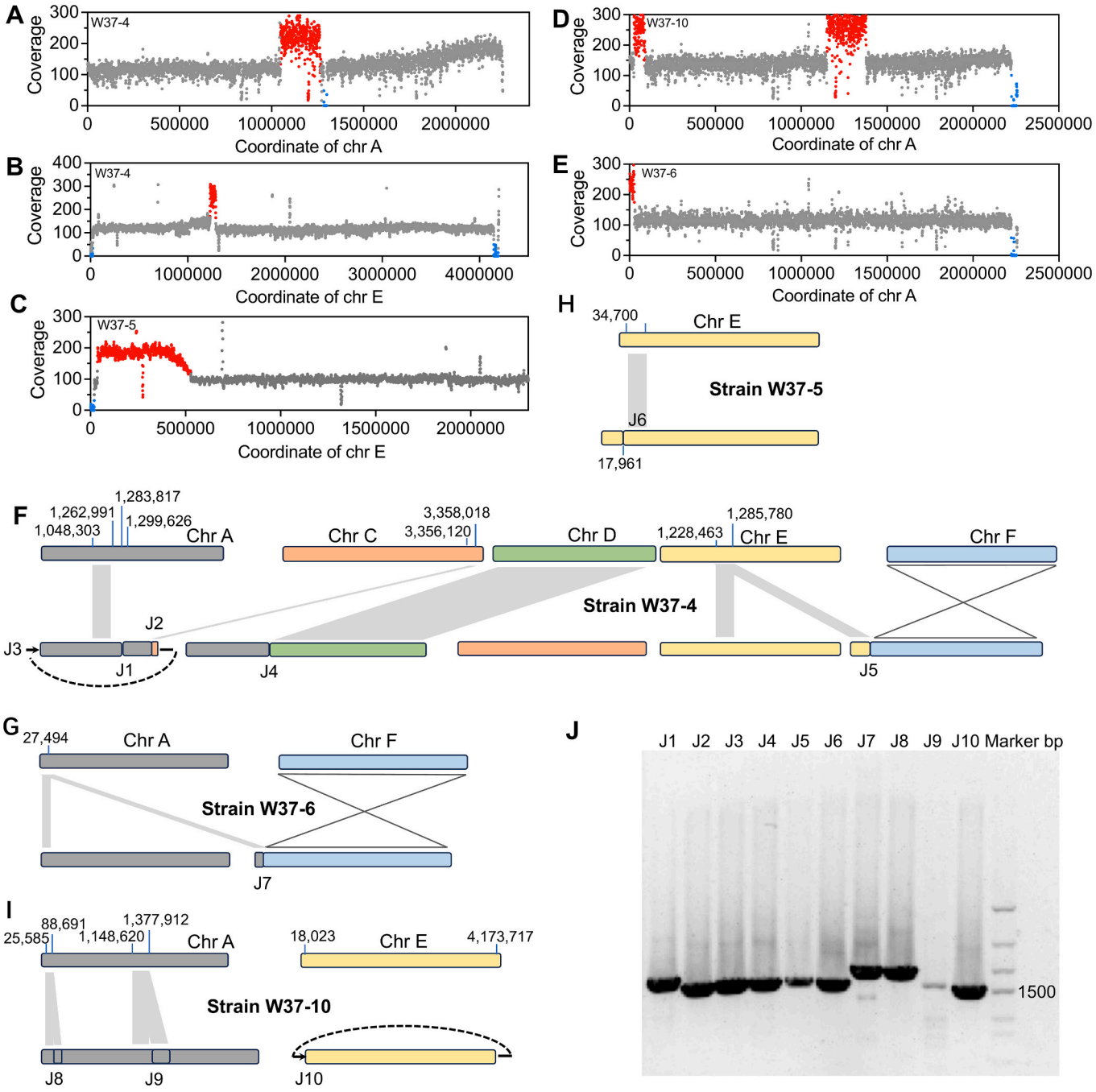


**Fig. 4.** High temperature induced large-scale chromosomal rearrangements in *Y. lipolytica*. (A-E) Sequencing coverage of certain chromosomes in several isolates subcultured under 37°C. The red and blue points indicate duplicated and deleted regions, respectively. Chromosomal rearrangements in the subcultured isolates (F) W37-4. (G) W37-10. (H) W37-5. (I) W37-6. Translocations are highlighted by gray rectangles, inversions by open double-triangles, and chromosomal circularization (head-to-tail joining) by dashed lines. J1-J10 indicated that rearrangement junctions. (J) Verification of chromosomal rearrangements events by PCR and agarose gel electrophoresis. The PCR products were analyzed by Sanger sequencing.

isolates (W37-4, W37-5, W37-6, and W37-10) using Oxford Nanopore technology (the N50 of reads was up to 11.3 kb). Analysis of chimeric (split) long reads enabled the precise mapping of chromosomal breakpoints for all previously identified variants (Fig. 4F-4I and Dataset S6). In strain W37-4, the duplicated 214 kb segment from chromosome A was found to be translocated and integrated at position 1,283,817 bp on the same chromosome (Fig. 4F and Dataset S6). Furthermore, the breakpoint at 1,299,626 bp on chromosome A was joined to the distal end of chromosome D. Intriguingly, a 1.28 Mb segment of chromosome A, fused with a minor fragment from chromosome C, underwent head-to-tail ligation to form a circular chromosome (Fig. 4F and Dataset S6). A parallel chromosome circularization event involving chromosome E was observed in strain W37-10 (Fig. 4G and Dataset S6). In strains W37-5 and W37-6, all amplified regions were localized near telomeres and, notably, each was fused to the terminus of a heterologous chromosome (Fig. 4H, I and Dataset S6). The junctions of these rearrangements were also confirmed by PCR and Sanger sequencing (Fig. 4J and Dataset S6). Taken together, the high frequency of circular chromosome formation and terminal fusions underscores a state of severe telomere instability induced by thermal stress. These mechanisms—comprising chromosome end-to-end joining and recombination-mediated subtelomeric fusion—likely represent a critical genetic response to mitigate telomere dysfunction, potentially facilitating yeast survival under extreme temperature conditions.

In *S. cerevisiae*, thermal stress has been inextricably linked to loss of heterozygosity (LOH) and aneuploidy (Shen et al., 2020), indicating that heat shock both triggers DNA breaks and disrupts faithful chromosomal disjunction. In contrast, the prevalence of circular chromosomes in *Y. lipolytica* underscores a distinct genomic strategy in response to telomere dysfunction. Heat stress likely induces telomere uncapping or the progressive degradation of telomeric repeats, necessitating "salvage" pathways—primarily mediated by NHEJ or break-induced replication (Kramara et al., 2018) —to execute head-to-tail ligations and terminal fusions. Although such radical rearrangements are often deleterious, the resultant rapid accumulation of CNVs events, such as the Mb-scale duplications observed on chromosomes A and E, creates a vast reservoir of genetic diversity. While the role of large-scale CNVs in environmental adaptation is well-documented in *S. cerevisiae* (Chen et al., 2025; Zheng et al., 2017; Zhu et al., 2024), the direct validation of specific CNVs-associated phenotypes remains unexplored in *Y. lipolytica*. Addressing this gap necessitates the future development of advanced large-fragment DNA manipulation tools to enable the precise and synthetic reconstruction of targeted CNVs events.

An intriguing question is whether these evolved strains harboring CNVs maintain genomic stability when reverted to optimal growth temperatures or subjected to other industrial conditions. Mechanistically, due to the presence of massive segmental duplications, strains carrying large-scale genomic amplifications are theoretically poised to exhibit higher baseline genomic instability than the wild-type parental strain. Furthermore, whether chromosome circularization compromises faithful mitotic segregation remains an open question; if it does, the propensity for whole-chromosome aberrations would logically escalate during cell division. Ultimately, a rigorous, quantitative comparison of genomic stability between these evolved variants and the wild-type strain awaits future long-term MA experiments.

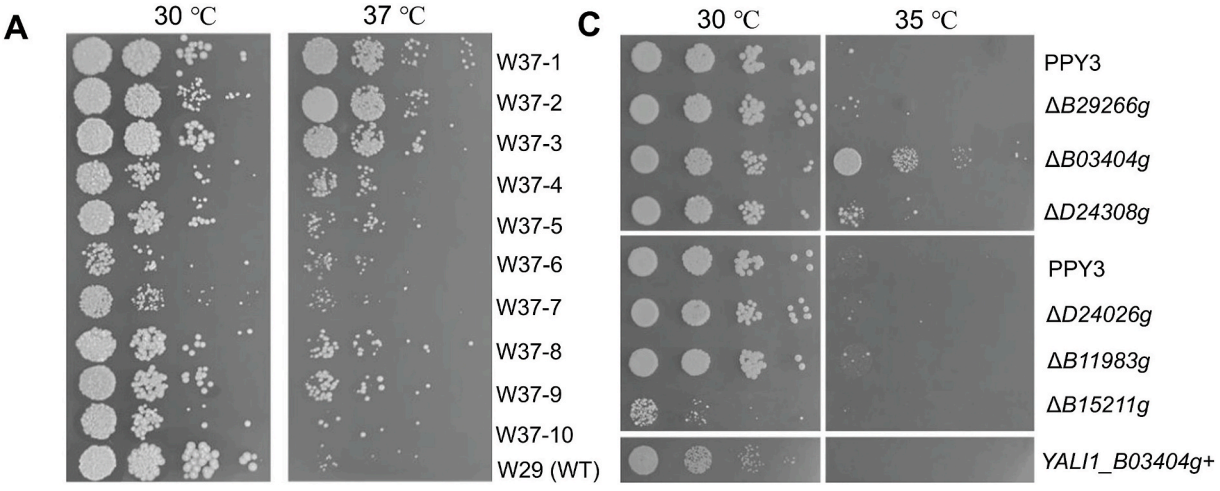


B

| Gene | Location | Reference | Mutation | Isolate |
|---|---|---|---|---|
| *YALI1_B29266g* | 2927940 | TC | T | W37-3 |
| *YALI1_B03404g* | 339769 | AT | A | W37-2 |
| *YALI1_D24308g* | 2430223 | TG | T | W37-1 |
| *YALI1_D24026g* | 2397300 | AG | A | W37-3 |
| *YALI1_B11983g* | 1198840 | C | T | W37-1 |
| *YALI1_E15211g* | 1520416 | TC | T | W37-3 |

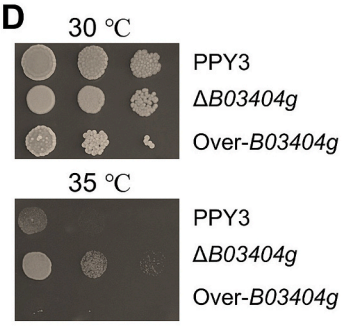


**Fig. 5.** Contribution of certain mutations to thermotolerance of *Y. lipolytica*. (A) Comparison of growth of the parental strain W29 and subcultured isolates under 30°C and 37°C. (B) Subset of mutations detected in the three subcultured isolates with higher thermotolerance. (C) Deletion of gene *YALI1_B03404g* led to an improved resistance to high temperature in *Y. lipolytica*. At the bottom of the panel, the complementation of *YALI1_B03404g* is shown to restore the heat-sensitive phenotype in the *YALI1_B03404g* deletion strain. (D) Growth comparison of *YALI1_B03404g* deletion and overexpression (strain PPFB03404g in Table 1) mutants versus the wild-type strain PPY3 cultured on YPD medium at 30°C and 37°C.

### 3.5. Deactivation of YALI1_B03404g confers enhanced thermotolerance in Y. lipolytica

Having established that thermal stress significantly accelerates mutagenesis, we next investigated how these genetic alterations modulate heat tolerance. A spotting assay revealed that three of the ten evolved isolates (W37-1–3) exhibited superior growth compared to the parental strain when cultured at 37°C (Fig. 5A). Whole-genome sequencing identified 13 frameshift-inducing InDels and 24 non-synonymous SNVs across these thermotolerant isolates (Datasets S2, S3). Given that frameshift mutations typically result in a complete loss of gene function, we hypothesized that the deactivation of specific genes might be the primary driver of the observed adaptive thermotolerance. To test this, we randomly selected 5 genes with frameshift mutations and 1 gene with an amino acid substitution mutation (Fig. 5B) for knockout and phenotypic verification in the parental strain PPY3 (a derivative of PO1f; Table 1) and evaluated their growth under thermal stress. Deletions of *YALI1_B20319g*, *YALI1_D24026g*, *YALI1_B11983g*, and *YALI1_D24308g* yielded no discernible impact on fitness at either 30°C or 35°C (Fig. 5C). In contrast, the loss of *YALI1_E15211g*—the homolog of *S. cerevisiae CSM3*, which encodes a subunit of the Tof1-Mrc1-Csm3 replication-pausing checkpoint complex—severely compromised cell viability even at 30°C, underscoring its essential role in maintaining normal growth (Fig. 5C).

We identified *YALI1_B03404g* as a critical locus for heat resistance after observing that its complete deletion significantly boosted *Y. lipolytica* growth under thermal stress (Fig. 5C). This mirrors the natural deactivation of the gene seen in the heat-tolerant isolate W37-2 (Fig. 5B). To validate this causal relationship, we performed a complementation assay; restoring the functional gene abolished the mutant's thermotolerance, thereby definitively linking the loss of *YALI1_B03404g* to the yeast's enhanced heat resistance. In contrast to the phenotypic effects of gene deletion, *YALI1_B03404g* overexpression resulted in more severe growth inhibition under high-temperature conditions in Y. lipolytica compared with the wild-type strain (Fig. 5D).

### 3.6. Functional investigation of YALI1_B03404g in Y. lipolytica

The protein encoded by *YALI1_B03404g* consists of 961 amino acids and possesses a distinct modular architecture (Fig. 6A). Its *N*-terminal region (residues 2–131) is characterized by a high density of glutamine, proline, and histidine residues. This is followed by a conserved HMG-

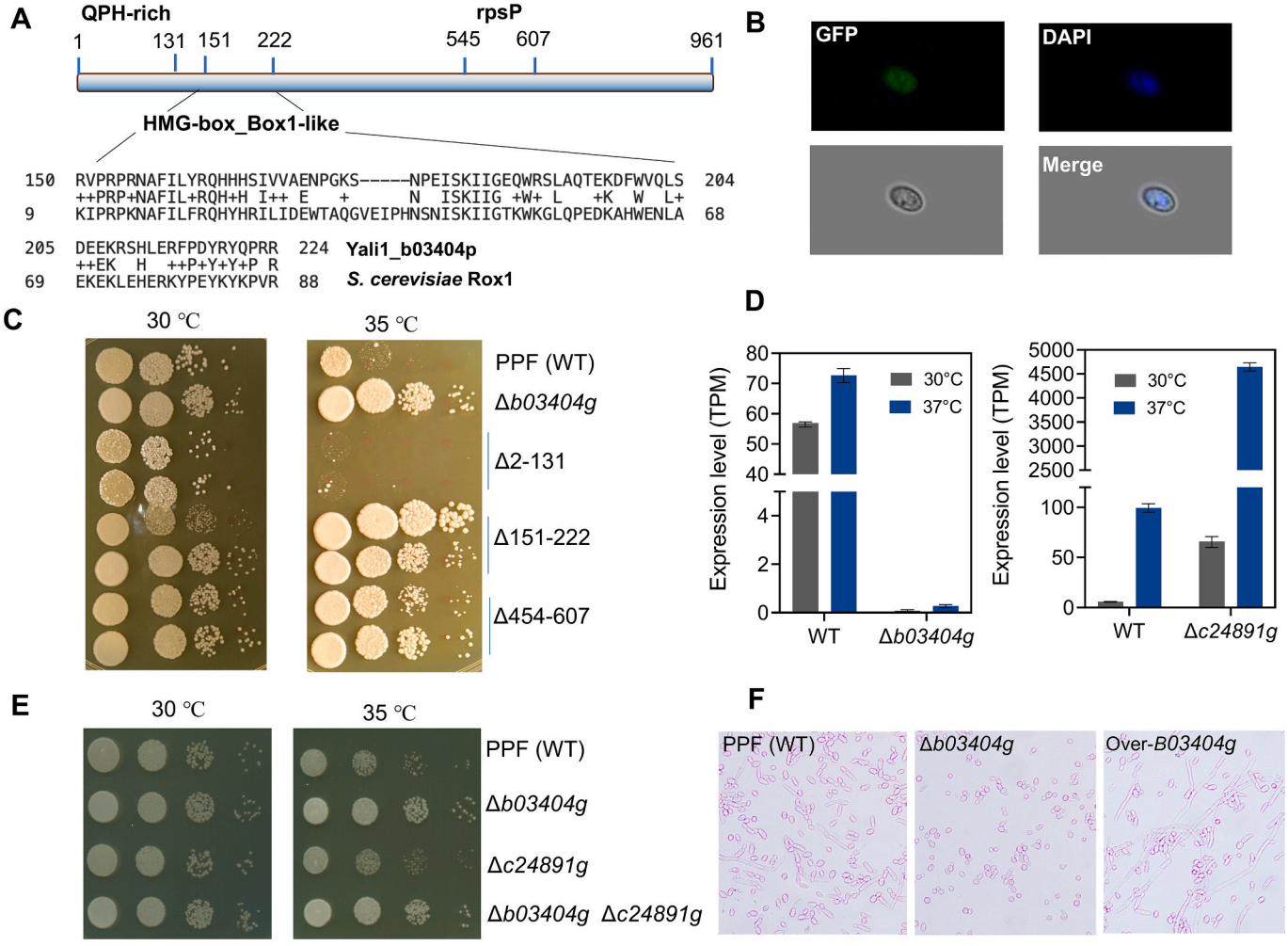


**Fig. 6.** Functional exploration of gene *YALI1_B03404g*. (A) In silico prediction of the domain architecture of the Yali1_b03404p protein. (B) Subcellular localization of the protein Yali1_b03404p-YFP. Nuclei were stained with DAPI. (C) Comparative growth assays evaluating the thermotolerance of the WT, the *YALI1_B03404g* deletion strain, and variants harboring domain-specific truncations. (D) mRNA expression level of *YALI1_B03404g* and *YALI1_C24891g* under 30°C and 37°C in both wild-type and Δ*yali1_b03404g* strains. (E) Phenotypic assessment showing that the deletion of *YALI1_C24891g* (encoding Ddr48-like protein) does not compromise the thermotolerance of *Y. lipolytica*. (F) Deletion of *YALI1_B03404g* represses the yeast-to- hypha transition, whereas overexpression of this gene promotes this morphological transformation. Cell morphology of the wild-type strain (PPF), the Δyali1_b03404g deletion mutant, and the *YALI1_B03404g* overexpression strain were obseved after 30 h of incubation on YPD plates.

box_ROX1-like motif (residues 151–222), which is typically associated with DNA binding and transcriptional regulation. Additionally, a central domain (residues 545–607) exhibits significant homology to the 30S ribosomal protein S16 (rpsP) (Fig. 6A). While the presence of an HMG-box_ROX1-like motif suggests a role as a DNA-binding transcription factor, subcellular localization analysis revealed that Yali1_b03404p does not exhibit the characteristic nuclear enrichment typically observed for conventional transcription factors (Fig. 6B). In *S. cerevisiae*, Rox1p is a well-known repressor of hypoxic genes. To delineate the functional contribution of these individual domains to thermal stress resistance, we generated three truncated variants of *YALI1_B03404g* lacking the *N*-terminal disordered region (Δ2-131), the HMG-box motif (Δ151-222), and the rpsP-like domain (Δ454-607), respectively. Phenotypic assays demonstrated that the 2–131 mutant maintained a heat-sensitive phenotype comparable to the wild-type strain (Fig. 6C). In stark contrast, the targeted deletion of either the HMG-box_ROX1-like motif or the rpsP-like domain significantly enhanced the thermotolerance of *Y. lipolytica*. These results suggest that Yali1_b03404p likely functions as a negative regulator of the heat stress response, with its DNA-binding and ribosomal-homology domains being essential for maintaining this inhibitory effect.

We also performed RNA-seq to explore the effect of *YALI1_B03404g* deletion on the transcriptome. Under standard (30°C) and elevated (37°C) temperatures (treated for 2 h), the mutant exhibited differential expression of a select set of genes: 16 and 19 genes were significantly upregulated, while 49 and 9 genes were downregulated at 30°C and 37°C, respectively (fold change $> 2$, $P < 0.01$; Dataset S5). Notably, although the deactivation of *YALI1_B03404g* promotes thermotolerance in the wild-type strain, its mRNA expression was slightly elevated upon exposure to 37°C (Fig. 6D). Among the differentially expressed genes, *YALI1_C24891g* stood out with a striking 11.6-fold and 70.6-fold upregulation in the Δ*yali1_b03404g* mutant at 30°C and 37°C, respectively (Fig. 6D). This suggests that *YALI1_B03404g* may function as a specific transcriptional repressor of *YALI1_C24891g*. The *S. cerevisiae* homolog of this gene is *DDR48*, which encodes a DNA damage-responsive protein induced by heat shock and genotoxic stress. *DDR48* is characterized by multiple conserved NNNDSYGS motifs, which are implicated in post-transcriptional regulation and the formation of stress granules. However, functional assays revealed that the deletion of *YALI1_C24891g* in *Y. lipolytica* did not alter its thermal resistance (Fig. 6E). Furthermore, the Δ*yali1_b03404g* Δ*yali1_c24891g* double mutant maintained a high-temperature tolerance level comparable to that of the Δ*yali1_b03404g* single mutant (Fig. 6E). Collectively, these results indicate that while the Ddr48-like protein is a major downstream target of *YALI1_B03404g* regulation, its massive induction is not the driver of the enhanced thermotolerance observed in the Δ*yali1_b03404g* strain.

Dimorphism (yeast-to-hypha transition) is a widespread trait among ascomycetous yeasts, having been most extensively characterized in *S. cerevisiae* and the opportunistic pathogen *Candida albicans*. In these species, the morphogenetic switch to hyphal growth serves as a fundamental adaptation, particularly for *C. albicans* where it is a critical determinant of infectious virulence and tissue invasion (Mitchell, 1998). Transcriptomic profiling of the Δ*yali1_b03404g* mutant at 30°C revealed 49 significantly downregulated genes, notably including the homeobox transcription factor Hoy1 (*YALI1_A19220g*) and a septin (*YALI1_F12578g*) encoding gene (Dataset S5), both of which are essential for hyphal development in *Y. lipolytica* (Oh and Bi, 2011; Torres-Guzmán and Domínguez, 1997). These results indicate that the loss of *YALI1_B03404g* recalibrates the morphogenetic landscape of *Y. lipolytica*. Consistent with these transcriptional shifts, the Δ*yali1_b03404g* mutant exhibited a constitutively higher proportion of yeast-form cells compared to the wild-type when cultured on solid media for 30 h (Fig. 6F). In contrast, strains overexpressing *YALI1_B03404g* exhibited a higher proportion of hyphal cells and displayed significantly increased filament length compared with the wild-type control (Fig. 6F). This phenotypic divergence suggests that *YALI1_B03404g* is critical for sensing nutrient-depletion signals and subsequently orchestrating the filamentous growth program. Importantly, this morphological arrest may provide a potential mechanistic link to the observed enhancement in thermotolerance. By suppressing filamentation, the Δ*yali1_b03404g* strain likely prioritizes metabolic resource allocation toward cell divisions under heat stress and maintains the structurally robust cell wall architecture characteristic of yeast-form cells.

## 4. Conclusion

This study investigates thermal stress-induced genomic instability and thermotolerance mechanisms in the oleaginous yeast Y. lipolytica, a promising industrial chassis limited by temperature sensitivity. At 37°C, SNVs and InDels increase 29-fold and 68-fold, respectively, compared to 30°C. The TLS DNA polymerases and NHEJ pathway were not attributed to heat induced mutations. Instead, this mutagenesis arises from compromised DNA polymerase fidelity and an overwhelmed mismatch repair system. Long-read sequencing reveals severe telomere instability, large-scale chromosomal rearrangements, and frequent circular chromosome formation under heat stress. We performed functional validation of mutation sites in evolved thermotolerant isolates and verified the roles of candidate genes via gene knockout and complementation assays. YALI1_B03404g is confirmed as a critical negative regulator of thermotolerance; it also regulates yeast-to-hypha transition, and its deletion strongly enhances heat resistance. These findings clarify how thermal stress drives rapid genomic diversification in non-conventional yeasts, deepen understanding of stress-driven genome evolution, and provide valuable genetic targets for engineering robust, thermotolerant microbial cell factories to improve industrial bioproduction efficiency.

## Ethical approval

This article does not contain any studies with human participants or animals performed by any of the authors.

## CRediT authorship contribution statement

**Min He:** Writing – original draft, Methodology, Data curation, Conceptualization. **Ke Zhang:** Writing – original draft, Resources, Funding acquisition, Data curation, Conceptualization. **Qian-Xin Hong:** Investigation, Data curation. **Yuan-Chun Fang:** Resources, Methodology. **Yuan-Ru Xiong:** Methodology, Data curation. **Ye-Ke Wang:** Methodology, Formal analysis, Data curation. **Dao-Qiong Zheng:** Writing – review & editing, Supervision, Investigation, Funding acquisition, Data curation, Conceptualization.

## Declaration of competing interest

The authors declare that they have no known competing financial interests or personal relationships that could have appeared to influence the work reported in this paper.

## Acknowledgement

This study was supported by grants from the National Natural Science Foundation of Zhejiang Province, China (LZ24C010002); and the National Natural Science Foundation of China (32270086 and 32170078).

## Appendix A. Supplementary data

Supplementary data to this article can be found online at https://doi.org/10.1016/j.biortech.2026.135071.

## Data availability

Data will be made available on request.

## References


Arbel, M., Liefshitz, B., Kupiec, M., 2021. DNA damage bypass pathways and their effect on mutagenesis in yeast. FEMS Microbiol. Rev. 45, fuaa038.

Bankar, A.V., Kumar, A.R., Zinjarde, S.S., 2009. Environmental and industrial applications of Yarrowia lipolytica. Appl. Microbiol. Biotechnol. 84, 847–865.

Bolger, A.M., Lohse, M., Usadel, B., 2014. Trimmomatic: a flexible trimmer for Illumina sequence data. Bioinformatics 30, 2114–2120.

Carratù, L., Franceschelli, S., Pardini, C.L., Kobayashi, G.S., Horvath, I., Vigh, L., et al., 1996. Membrane lipid perturbation modifies the set point of the temperature of heat shock response in yeast. PNAS 93, 3870–3875.

Chen, G., Shan, Y., Wang, J., Zhang, Q., Yao, L., Chen, X., 2025. Multiple lignocellulosic inhibitor-tolerant Saccharomyces cerevisiae strains developed by evolutionary engineering and CRISPR/Cas9 gene editing technology. J. Agric. Food Chem. 73, 23486–23497.

Cingolani, P., Platts, A., Wang, L.L., Coon, M., Nguyen, T., Wang, L., et al., 2012. A program for annotating and predicting the effects of single nucleotide polymorphisms, SnpEff: SNPs in the genome of Drosophila melanogaster strain w1118; iso-2; iso-3. Fly 6, 80–92.

Davidson, J.F., Whyte, B., Bissinger, P.H., Schiestl, R.H., 1996. Oxidative stress is involved in heat-induced cell death in Saccharomyces cerevisiae. PNAS 93, 5116–5121.

Dobin, A., Davis, C.A., Schlesinger, F., Drenkow, J., Zaleski, C., Jha, S., et al., 2013. STAR: ultrafast universal RNA-seq aligner. Bioinformatics 29, 15–21.

Elliott, B., Haltiwanger, R.S., Futcher, B., 1996. Synergy between trehalose and Hsp104 for thermotolerance in Saccharomyces cerevisiae. Genetics 144, 923–933.

Fraczek, M.G., Naseeb, S., Delneri, D., 2018. History of genome editing in yeast. Yeast 35, 361–368.

Grousl, T., Ivanov, P., Malcova, I., Pompach, P., Frydlova, I., Slaba, R., et al., 2013. Heat shock-induced accumulation of translation elongation and termination factors precedes assembly of stress granules in S. cerevisiae. PLoS One 8, e57083.

Gusa, A., Yadav, V., Roth, C., Williams, J.D., Shouse, E.M., Magwene, P., et al., 2023. Genome-wide analysis of heat stress-stimulated transposon mobility in the human fungal pathogen Cryptococcus deneoformans. PNAS 120, e2209831120.

Habibi, P., Ostad, S.N., Heydari, A., Aliebrahimi, S., Montazeri, V., Foroushani, A.R., et al., 2022. Effect of heat stress on DNA damage: a systematic literature review. Int. J. Biometeorol. 66, 2147–2158.

Huang, C.J., Lu, M.Y., Chang, Y.W., Li, W.H., 2018. Experimental evolution of yeast for high-temperature tolerance. Mol. Biol. Evol. 35, 1823–1839.

Jenkins, G.M., Richards, A., Wahl, T., Mao, C., Obeid, L., Hannun, Y., 1997. Involvement of yeast sphingolipids in the heat stress response of Saccharomyces cerevisiae. J. Biol. Chem. 272, 32566–32573.

Koboldt, D.C., Zhang, Q., Larson, D.E., Shen, D., McLellan, M.D., Lin, L., et al., 2012. VarScan 2: somatic mutation and copy number alteration discovery in cancer by exome sequencing. Genome Res. 22, 568–576.

Kramara, J., Osia, B., Malkova, A., 2018. Break-induced replication: the where, the why, and the how. Trends Genet. 34, 518–531.

Li, H., 2013. Aligning sequence reads, clone sequences and assembly contigs with BWA-MEM. arXiv; arXiv:1303.3997.

Li, H., Handsaker, B., Wysoker, A., Fennell, T., Ruan, J., Homer, N., et al., 2009. The sequence alignment/map format and SAMtools. Bioinformatics 25, 2078–2079.

Liang, P., Li, J., Wang, Q., Dai, Z., 2023. Enhancing the thermotolerance and erythritol production of Yarrowia lipolytica by introducing heat-resistant devices. Front. Bioeng. Biotechnol. 11, 1108653.

Liao, Y., Smyth, G.K., Shi, W., 2014. featureCounts: an efficient general purpose program for assigning sequence reads to genomic features. Bioinformatics 30, 923–930.

Liu, M., Cheng, H., 2023. Discovery and functional evaluation of heat tolerance genes in the nonconventional yeast Yarrowia lipolytica. Fermentation 9, 509.

Love, M.I., Huber, W., Anders, S., 2014. Moderated estimation of fold change and dispersion for RNA-seq with DESeq2. Genome Biol. 15, 550.

Mitchell, A.P., 1998. Dimorphism and virulence in Candida albicans. Curr. Opin. Microbiol. 1, 687–692.

Mitra, S., Boldogh, I., Izumi, T., Hazra, T.K., 2001. Complexities of the DNA base excision repair pathway for repair of oxidative DNA damage. Environ. Mol. Mutagen. 38, 180–190.

Oh, Y., Bi, E., 2011. Septin structure and function in yeast and beyond. Trends Cell Biol. 21, 141–148.

Pereira, T., Vilaprinyo, E., Belli, G., Herrero, E., Salvado, B., Sorribas, A., et al., 2018. Quantitative operating principles of yeast metabolism during adaptation to heat stress. Cell Rep. 22, 2421–2431.

Qin, J., Liu, N., Abid, U., Coleman, S.M., Wang, Y., Fu, Q., et al., 2025. Metabolic engineering of Yarrowia lipolytica for conversion of waste cooking oil into omega-3 eicosapentaenoic acid. ACS Eng. Au 5, 128–139.

Qiu, X., Gu, Y., Du, G., Zhang, J., Xu, P., Li, J., 2021. Conferring thermotolerant phenotype to wild-type Yarrowia lipolytica improves cell growth and erythritol production. Biotechnol. Bioeng. 118, 3117–3127.

Quinlan, A.R., Hall, I.M., 2010. BEDTools: a flexible suite of utilities for comparing genomic features. Bioinformatics 26, 841–842.

Shahsavarani, H., Sugiyama, M., Kaneko, Y., Chuenchit, B., Harashima, S., 2012. Superior thermotolerance of Saccharomyces cerevisiae for efficient bioethanol fermentation can be achieved by overexpression of RSP5 ubiquitin ligase. Biotechnol. Adv. 30, 1289–1300.

Shen, L., Wang, Y.T., Tang, X.X., Zhang, K., Wang, P.M., Sui, Y., et al., 2020. Heat shock drives genomic instability and phenotypic variations in yeast. AMB Express 10, 146.

Torres-Guzmán, J.C., Domínguez, A., 1997. HOY1, a homeo gene required for hyphal formation in Yarrowia lipolytica. Mol. Cell Biol. 17, 6283–6293.

Wang, N., Chi, P., Zou, Y., Xu, Y., Xu, S., Bilal, M., et al., 2020. Metabolic engineering of Yarrowia lipolytica for thermoresistance and enhanced erythritol productivity. Biotechnol. Biofuels 13, 176.

Xiong, Y.R., Fang, Y.C., He, M., Li, K.J., Qi, L., Sui, Y., et al., 2025. Patterns of spontaneous and induced genomic alterations in Yarrowia lipolytica. Appl. Environ. Microbiol. 89, e01678–e01724.

Xu, L., Nitika, H.N., Cuskelly, D.D., Wolfgeher, D., Doyle, S., et al., 2019. Rapid deacetylation of yeast Hsp70 mediates the cellular response to heat stress. Sci. Rep. 9, 16260.

Yan, C., Wang, Y.K., Xiong, Y.R., Zhou, X.Q., Fang, Y.C., Nie, R.T., et al., 2025. The roles of NHEJ and TLS pathways in genomic alterations and phenotypic evolution in the yeast Yarrowia lipolytica. Appl. Microbiol. Biotechnol. 109, 183.

Yook, S., Deewan, A., Ziolkowski, L., Lane, S., Tohidifar, P., Cheng, M.H., et al., 2025. Engineering and evolution of Yarrowia lipolytica for producing lipids from lignocellulosic hydrolysates. Bioresour. Technol. 416, 131806.

Zhang, Y., Zhang, X., Xu, Y., Xu, S., Bilal, M., Cheng, H., 2022. Engineering thermotolerant Yarrowia lipolytica for sustainable biosynthesis of mannitol and fructooligosaccharides. Biochem. Eng. J. 187, 108604.

Zheng, D.Q., Jin, X.N., Zhang, K., Fang, Y.H., Wu, X.C., 2017. Novel strategy to improve vanillin tolerance and ethanol fermentation performances of Saccharomyces cerevisiae strains. Bioresour. Technol. 231, 53–58.

Zheng, D.Q., Wang, Y.T., Zhu, Y.X., Sheng, H., Li, K.J., Sui, Y., et al., 2022. Uncovering bleomycin-induced genomic alterations and underlying mechanisms in the yeast Saccharomyces cerevisiae. Appl. Environ. Microbiol. 88, e01703–e01721.

Zhou, T., Park, Y.K., Fu, J., Hapeta, P., Klemm, C., Ledesma-Amaro, R., 2025. Metabolic engineering of Yarrowia lipolytica for the production and secretion of the saffron ingredient crocetin. Biotechnol Biofuels Bioproducts 18, 1.

Zhu, Y.X., He, M., Li, K.J., Wang, Y.K., Qian, N., Wang, Z.F., et al., 2024. Novel insights into the effects of 5-hydroxymethfurural on genomic instability and phenotypic evolution using a yeast model. Appl. Environ. Microbiol. 90, e01649–e01723.